# A Horizontal Accuracy Metric for Magnetic Navigation

## 1 Introduction

Magnetic Navigation (MagNav) is a rising form of alternative navigation which uses a map of the Earths crustal magnetic field over a given area of interest and compares the mapped value at an initial estimate of the position to the measured output of a quantum magnetometer in order to update the estimate.

The crustal field (or anomaly field) of the Earth is a result of permanent or induced magnetization in the crust and has a magnitude of the order of 100 nT with a spatial variation of 200 nT at approximately 1 km height above terrain (Gnadt, 2022a). While the magnitude of the crustal field is much smaller in comparison with the Earth's core field (approximately 50,000 nT), the local variation and the relative temporal stability of the field (approximately 1 nT per year) makes the crustal field suitable for navigation, when using sensitive magnetic scalar and vector sensors. An extensive background and history of the MagNav problem is provided in Canciani and Raquet (2016). This reference also shows that a navigation accuracy of up to 13 m can be achieved using a combination of a marginalized particle filter, high-quality magnetic anomaly map, and low flight altitudes. The focus of MagNav has generally been on the defense domain (Canciani, 2022), although there is new interest in its application for civil aviation as a means of protection against jamming and spoofing of Global Navigation Satellite Systems (GNSS).

Navigation in the civil aviation context requires discussing the notion of accuracy. A definition of accuracy is provided by the Area Navigation (RNAV) and Required Navigation Performance (RNP) specifications that are defined as part of Performance Based Navigation (PBN) (Federal Aviation Administration, 2024). More specifically, Federal Aviation Administration (2024) states that "For both RNP and RNAV designations, the numerical designation refers to the lateral navigation accuracy in nautical miles which is expected to be achieved at least 95 percent of the flight time by the population of aircraft operating within the airspace, route, or procedure." In the present work, RNAV and RNP are used interchangeably for navigation accuracy definitions, although it is acknowledged that RNP also requires a notion of integrity and continuity, both of which are beyond the scope of discussion for magnetic navigation.

Functionally, for a system which uses a filter to estimate an aircraft's position, either by using signals-in-space such as the Global Positioning System (GPS) (SC-159, 2020a, 2020b) or by using a combination of Navigation Aids (NAVAIDs) such as Very High Frequency Omnidirectional Range (VOR) and Distance Measuring Equipment (DME) (Federal Aviation Administration, 2024), this

translates to showing that the uncertainty in the lateral or cross-track error, characterized by a standard deviation, is less than a given threshold.

In "ICAO Doc 9613, Performance-based Navigation (PBN) Manual" (2023), it is noted that currently there are no specifications for longitudinal error, with the exception of Navigation System Error (Section 2.2.2), other than for RNP 4 (Part C). The requirement for longitudinal accuracy is also discussed in the context of future specifications in Section 1.6. It is also noted in Section 2.3.3.3 that for monitoring and alerting purposes, some systems apply the limit to the standard deviation of each axis (cross-track and along-track) separately, whereas other systems apply the 95 percent limit to the combined (2D) radial error. The difference between a bound on single-axis errors as opposed to radial errors is nuanced because the error distribution along individual axes can be assumed to be Gaussian, but radial errors are non-negative and therefore are not Gaussian. For GPS-based or NAVAID-based positioning, the difference does not generally impact operations because the uncertainty introduced by both systems is not dependent on the direction of travel except for the higher latitudes for GPS, and areas where NAVAID density is poor.

The lack of directional sensitivity is furthermore noted in GPS-based navigation concepts. The definition of GPS Dilution of Precision (DOP) (Langley, 1999), evaluates the vertical accuracy (VDOP) and horizontal accuracy (HDOP) separately, but the HDOP is usually not decomposed further in either the North-East or longitudinal-lateral directions, although it can be, if the application requires it. For example, Satellite-Based Augmented System- (SBAS-) aided GPS uses the major principal axis variance when calculating the Horizontal Protection Level (HPL) for the position solution (SC-159, 2020a). Additionally, integrity monitoring using the Advanced Receiver Autonomous Integrity Monitoring (ARAIM) algorithm (Blanch et al., 2015) calculates the HPL using the norm of the HPL along the two horizontal axes, which implicitly assumes that both axes have the same error distribution.

In contrast, the impact of direction on positioning accuracy is significant for MagNav. A discussion of this impact is motivated by first examining the magnetic anomaly value over a given region of the Earth. In Figure 4, the magnetic anomaly measurement sourced from North American Magnetic Anomaly Group (2002) (NAMAM) is shown at two different altitudes (referenced to the ellipsoidal Earth): 1000 m and 4000 m. At higher altitudes, the measurable magnetic anomaly generally has a smaller magnitude, and smaller gradients, which will generally result in lower positioning accuracy from MagNav. However, strong directionality in the magnetic anomaly gradient, regardless of magnitude, can exhibit itself at any altitude.

This notion is further developed using Figures 1 through 3 on the left, where the gradient of magnetic anomaly is shown for three different heading values with respect to True North:, 0 degrees, 60 degrees, and 120 degrees. At any given point, the gradient is calculated with respect to the latitude and longitude at that point. In these figures, the two-dimensional gradient is projected onto the unit vector along the desired heading. In general, regions with high gradient magnitude are expected to result in better MagNav performance (accuracy) than regions with low gradient magnitude. In regions where the gradient magnitude is low, the magnetic anomaly does not change

significantly between two measurement updates, and the estimator is not able to infer how the current estimate should be updated. This is the classic observability problem that is encountered in any filtering application (Crassidis & Junkins, 2004).

A general overview of the magnetic anomaly gradient in Figures 1 through 3 (left) suggests that one should expect different gradient behavior in different directions. A natural question is the impact of the magnetic anomaly gradient on positioning accuracy as a function of heading. This impact can be determined by first characterizing the overall positioning accuracy achievable from a given map. For example, Tkhorenko and Karshakov (2022) evaluates the impact of upward continuation of magnetic anomaly map data on a static position estimate using Cramér-Rao Lower Bound (CRLB) analysis. In this context, "upward continuation" refers to stable extrapolation away from the magnetic anomaly source (Phillips, 2005). Gupta, Sengupta, Phernetton, and Sosanya (2024) considers a more general problem of directional dependency using a Bayesian CRLB analysis. This allows the translation of a magnetic anomaly map into a CRLB map as shown in Figure 1 (right), Figure 2 (right), and Figure 3 (right), where the gradient information is obtained from the magnetic anomaly map sourced from North American Magnetic Anomaly Group (2002). This gradient information is then used to calculate the Bayesian along-track CRLB along a straight path at headings of 0 degrees, 60 degrees, and 120 degrees, respectively, for an aircraft traveling at 85m/s at an altitude of 1000 m above an ellipsoidal Earth. It should be noted that the gradient itself may have an error in it due to error introduced by compiling different sources of data with varying quality. Some of these error sources are discussed in Saltus, Chulliat, Meyer, Bates, and Sirohey (2023). Considering that the CRLB itself is the lower bound on the position error, error in the gradient calculation is a second-order effect that can be captured by the overall measurement uncertainty.

The measurement uncertainty that is used in order to generate the CRLB plots shown in these figures is a combination of the error variance of the magnetometer measurement, error in the map, and calibration error due to electromagnetic interference from the airframe and the airframe interaction with the core field. The calibration error can dominate the other sources if sensors are not installed in areas isolated from electromagnetic interference. Calibration error is reduced using either first-order techniques such as Tolles-Lawson calibration (Gnadt, Wollaber, & Nielsen, 2022) or more-recent machine learning-based calibration (Gnadt (2022b); Zhai, Moradi, Kong, and Lai (2023); Moradi, Zhai, Nielsen, and Lai (2024)). For example, the work in Gnadt (2022b) suggests that the error can be reduced to approximately 5 nT, especially if sensors are located such that electromagnetic interference is minimized, and if maps are of good quality. The value of 25 nT captures the reduction in the calibration error achieved in recent work (Nerrise, Sosanya, & Neary, 2024) on the MagNav challenge data set (Gnadt et al., 2023), and that is the value used in this paper.

The CRLB value at a location specifies the best possible performance of a recursive filter used for navigation under the assumption of perfectly-known dynamics and a perfect inertial measurement unit providing bias-free accelerations. Therefore the CRLB value is a function of magnetic anomaly

information in a map, specifically its gradient. As evidenced by the CRLB map, the expected accuracy in different directions of travel can be significantly different. This is shown in Figure 5. In this figure, the points correspond to the CRLB along different directions and are calculated using the approach presented in Gupta et al. (2024). An ellipse is then fit through these points using least squares. While it is also possible to plot the two-dimensional ellipse corresponding to the CRLB covariance, the first approach removes any sensitivity to direction of flight and consequently better represents the relationship between the magnetic anomaly gradient direction and the expected navigation accuracy. In the present example, the ratio of principal axis standard deviations is approximately 0.4. While it is a useful endeavor to evaluate all possible values of this ratio for every mapped location, this is an intensive task because it requires evaluating CRLB over a range of altitudes, groundspeeds, and headings over large maps – either NAMAM for North America, or the Earth Magnetic Anomaly Grid (EMAG2) (Maus et al., 2009) for world-wide analysis. Consequently, this endeavor is considered beyond the scope of the paper. Instead the focus is on the certainty that the positioning error statistics will be mismatched and on the consequences of this mismatch.

As noted earlier, the standard deviations in Figure 5 correspond to a measurement uncertainty of 25 nT. If the measurement uncertainty is large (e.g. 100 nT), the radial asymmetry of the type shown here would continue to exist because gradient directions are not random. Consequently, over a relatively short interval of time, if the gradient direction shows little variation, the posterior variance in the direction of the gradient would continue to decrease, whereas the posterior variance in the direction normal to the gradient would be non-decreasing.

The foregoing observation motivates the study in this paper: even if the navigation accuracy specification is restricted to lateral errors, the use of MagNav can result in the following two divergences from the underlying assumptions:

1. The correlation coefficient between the longitudinal and lateral errors can be sufficiently high such that even if the marginal distribution in the lateral direction meets the specification, the true radial error can exceed the specification.

2. The difference in magnitude between lateral and longitudinal error uncertainty can result in an unintended separation violation in the along-track direction even when the cross-track specification is met.

The scenario discussed here is shown as a schematic diagram in Figure 6. In this figure, the shaded ellipse depicts the confidence bounds on a two-dimensional position error distribution where the error components follow a bivariate normal distribution. Even though the lateral accuracy bounds, denoted by the dashed lines, are satisfied by the 95% cross-track uncertainty bound, denoted by the dotted lines, it is still possible to violate a separation constraint with an aircraft that is outside this lateral bound, but slightly ahead to the right.

Conversely, studying the probability of exceedance for a radial metric instead of a lateral or cross-track metric can inform future considerations for increasing traffic density using MagNav.

This work proposes a reasonable metric for performance which meets the definition of accuracy under PBN. Furthermore it evaluates the gap between the current method of calculating accuracy and the metric proposed in the paper.

This paper is organized into the following sections. First, the general concept of accuracy is presented as used for current operations. Next, a new metric based on the general quadratic form (Provost & Mathai, 1992) is proposed, and it is shown how this metric can be calculated. Finally, results are shown that indicate how the new metric can benefit the establishment of tighter performance bounds under the definition of RNP accuracy and containment region.

## 2 Bounds on Accuracy and Probability of Exceedance

This section is concerned with the definition of horizontal navigation accuracy, namely, bounds on radial error when the individual components are stochastic. To this end, let $x$ and $y$ be the in-plane position errors in any coordinate frame (North and East, or Along-Track and Cross-Track). Typically $x$ and $y$ are expected to have a joint normal distribution where the marginal distributions have a standard deviation of $\sigma_x$ and $\sigma_y$ respectively. For the moment, it is assumed that the distribution is uncorrelated (in a later section the general problem of a correlated distribution will be considered). The radial error is denoted by $r$ and is given by $r = \sqrt{x^2 + y^2}$. This paper develops an answer to the following question: what values of $\sigma_x$ and $\sigma_y$ ensure that the probability that $r$ exceeding $r_t$ is no greater than $p_e$?

As noted earlier, Section 2.3.3.3 of "ICAO Doc 9613, Performance-based Navigation (PBN) Manual" (2023), suggests two alternative methods to calculate $\sigma_x$ and $\sigma_y$ corresponding to a given radial distance threshold. These are described in the following two subsections.

### 2.1 Radial Error lesser than Threshold

The requirement for navigation accuracy can be stated in terms of the probability density function of $r$, a distance error threshold $r_t$ and a probability of exceedance $p_e$ as the following statement:

$$p(r = \sqrt{x^2 + y^2} > r_t, \sigma_x, \sigma_y) = p_e \tag{1}$$

In other words, the probability that the radial error $r$ exceeds a threshold $r_t$ is equal to $p_e$ or lower, with the equality denoting the bounding case.

Since $\sqrt{x^2 + y^2}$ is non-negative, the foregoing equation can also be written as

$$p(\sqrt{x^2 + y^2} \leq r_t, \sigma_x, \sigma_y) = 1 - p_e \tag{2}$$

For example, the RNP definition requires that the error be less than the threshold for 95% of the flight time. Consequently, $p_e = 0.05$ when $r_t = r_{\text{RNP}}$.

Similarly, the containment region is defined such that the probability of exceeding $r_t = r_{\text{cont}}$ is lesser than $10^{-5}$ or $10^{-7}$ depending on the application. For the purposes of this paper, the

generalized requirement in (2) will be considered, while the RNP definition will be used as an example.

In terms of the cumulative density function, (2) is restated as follows:

$$\mathrm{CDF}(\sqrt{x^2+y^2} = r_t, \sigma_x, \sigma_y) = 1 - p_e \tag{3}$$

where $\mathrm{CDF}(\cdot)$ is the cumulative density function of the random variable $r = \sqrt{x^2+y^2}$.

Under the assumption of $\sigma_x = \sigma_y$, the probability density in (3) corresponds to the Rayleigh distribution, which is equivalent to the chi-square distribution with two degrees of freedom. The probability density function and cumulative density function of the Rayleigh distribution are respectively given by:

$$\mathrm{PDF}_{\mathrm{Rayleigh}}(r, \sigma) = \frac{r}{\sigma^2} \exp\left(-\frac{r^2}{2\sigma^2}\right) \tag{4}$$

$$\mathrm{CDF}_{\mathrm{Rayleigh}}(r, \sigma) = 1 - \exp\left(-\frac{r^2}{2\sigma^2}\right) \tag{5}$$

The general requirement for a threshold radius meeting a probability requirement under the assumptions of a Rayleigh distribution is given in terms of the following expression:

$$\mathrm{CDF}_{\mathrm{Rayleigh}}(r_t, \sigma) = 1 - \exp\left(-\frac{r_t^2}{2\sigma^2}\right) = 1 - p_e \tag{6}$$

which can be easily solved for $\sigma$ as shown below:

$$\sigma = \frac{r_t}{\sqrt{-2\log p_e}} \tag{7}$$

Since the RNP value formally requires that $r \leq \mathrm{RNP}$ with 95% probability, (7) is restated as follows:

$$\sigma_{\mathrm{RNP}} = \frac{r_{\mathrm{RNP}}}{\sqrt{-2\log p_{\mathrm{exceedance/RNP}}}} = \frac{r_{\mathrm{RNP}}}{\sqrt{-2\log 0.05}} \approx 0.408\, r_{\mathrm{RNP}} \tag{8}$$

## 2.2 Individual Axis Errors lesser than Threshold

Let $z$ denote the two dimensional vector with components $x$ and $y$. It is observed that $r = \sqrt{x^2+y^2} = ||z||_2$, where $||\cdot||_2$ denotes the 2-norm of the vector. Using the norm inequality relationship between the 2-norm and $\infty$-norm, $||z||_2 \geq ||z||_\infty$ where $||z||_\infty = \max(|x|, |y|)$. Applying the condition on individual axis results in a redefinition of (2) into the following statement:

$$p(\max(|x|, |y|) \leq r_t, \sigma_x, \sigma_y) = 1 - p_e \tag{9}$$

Equation (9) is equivalent to the following:

$$p(|x| \leq r_t, |y| \leq r_t, \sigma_x, \sigma_y) = 1 - p_e \tag{10}$$

Equation (10) allows the use the zero-mean, uncorrelated bivariate normal distribution. This distribution is given by:

$$\mathrm{PDF}_{\mathrm{Bivariate}}(x, y, \sigma_x, \sigma_y) = \frac{1}{2\pi\,\sigma_x\sigma_y} \exp\left(-\frac{x^2}{2\sigma_x^2} - \frac{y^2}{2\sigma_y^2}\right) \tag{11}$$

From (11), (10) is calculated as follows:

$$\begin{aligned} p(|x| \leq r_t, |y| \leq r_t, \sigma_x, \sigma_y) &= \int_{y=-r_t}^{y=r_t} \int_{x=-r_t}^{x=r_t} \frac{1}{2\pi\,\sigma_x\sigma_y} \exp\left(-\frac{x^2}{2\sigma_x^2} - \frac{y^2}{2\sigma_y^2}\right) dx\,dy \\ &= \mathrm{erf}\left(\frac{r_t}{\sqrt{2}\,\sigma_x}\right) \mathrm{erf}\left(\frac{r_t}{\sqrt{2}\,\sigma_y}\right) \\ &= 1 - p_e \end{aligned} \tag{12}$$

where $\mathrm{erf}(\cdot)$ is the error function (Abramowitz & Stegun, 1972, p. 296).

Under the assumption that $\sigma_x = \sigma_y$, (12) can be solved as shown below:

$$\sigma = \frac{r_t}{\sqrt{2}\,\mathrm{erf}^{-1}\left(\sqrt{1 - p_e}\right)} \tag{13}$$

As before, for a probability of exceedance equal to 0.05, the standard deviation limit that is allowed under RNP is approximately equal to

$$\sigma'_{\mathrm{RNP}} = \frac{r_{\mathrm{RNP}}}{\sqrt{2}\,\mathrm{erf}^{-1}\left(\sqrt{1 - 0.05}\right)} \approx 0.447 r_{\mathrm{RNP}} \tag{14}$$

Upon comparing (14) to (8) it is evident that applying the RNP criterion to position accuracy along individual axes allows for approximately a 9% increment over the application of the RNP criterion to the radial accuracy. However, they are both generally conservative bounds on the actual probability of exceedance of the radial error. This is because these methods assume that the standard deviation of the error distribution along are equal, and if they are not equal, the larger of the two must be used in order for the assumption to hold. As noted earlier, this assumption has shown to not hold for MagNav specifically. In the next section, the general problem of unequal standard deviations is analyzed.

# 3 Navigation Accuracy using Quadratic Forms on Random Variables

The general case of a two-dimensional position error vector where $x$ and $y$ have a joint normal distribution is considered here. As before, the marginal distributions have a standard deviation of $\sigma_x$ and $\sigma_y$ respectively. Additionally, the distribution of the two-dimensional position error has a generally non-zero correlation coefficient denoted $\rho$. The covariance matrix is denoted by:

$$P = \begin{bmatrix} \sigma_x^2 & \rho\sigma_x\sigma_y \\ \rho\sigma_x\sigma_y & \sigma_y^2 \end{bmatrix} \tag{15}$$

Using the spectral decomposition theorem (Provost & Mathai, 1992), one can write $P = VDV^\top$ where $V$ is the matrix composed of the eigenvectors of $P$ and $D$ is a diagonal matrix whose entries are the eigenvalues of $P$. The matrix $V$ defines a rotation from the frame of rotation in which $x$ and $y$ are defined, into a frame of reference aligned with the uncertainty ellipsoid corresponding to the normal distribution with covariance matrix $P$.

Let $z' = V^{-1}z$, that is, $z'$ has coordinates in the principal axis frame. This new random vector is also normally distributed with covariance given by

$$\begin{aligned} E[z'z'^\top] &= E[V^{-1}zz^\top {V^{-1}}^\top] \\ &= V^{-1}E[zz^\top]{V^{-1}}^\top \\ &= V^{-1}P{V^{-1}}^\top \\ &= V^{-1}VDV^\top {V^{-1}}^\top \\ &= D \end{aligned} \tag{16}$$

It should be noted that $||z'|| = \sqrt{z'^\top z'} = \sqrt{z^\top V^\top V z} = \sqrt{z^\top z} = ||z||$, because $V^\top = V^{-1}$. Due to this rotation invariance, the probability density of $||z||$ whose covariance is given by a general positive definite matrix $P$ is equal to the probability density of $||z'||$ whose covariance is given by a diagonal matrix $D$, i.e. the variances of the new distribution are the eigenvalues of $P$. Therefore, without loss of generality, one can consider the distribution of $||z|| = \sqrt{x^2 + y^2}$ where $x$ and $y$ are uncorrelated normal distributions, whose standard deviations can be obtained from the eigenvalues of $P$, i.e. the diagonal elements of $D$. These eigenvalues are denoted by $\lambda_{\max}$ and $\lambda_{\min}$ respectively, and are given by:

$$\begin{aligned} \lambda_{\max} &= \frac{\sigma_x^2 + \sigma_y^2}{2} + \frac{1}{4}\sqrt{(\sigma_x^2 + \sigma_y^2)^2 - 4\sigma_x^2\sigma_y^2(1-\rho^2)} \\ \lambda_{\min} &= \frac{\sigma_x^2 + \sigma_y^2}{2} - \frac{1}{4}\sqrt{(\sigma_x^2 + \sigma_y^2)^2 - 4\sigma_x^2\sigma_y^2(1-\rho^2)} \end{aligned} \tag{17}$$

It should be noted that (17) assumes that $\sigma_x >= \sigma_y$.

When the standard deviations of $x$ and $y$ are different, denoted by $\sigma_x$ and $\sigma_y$ respectively, it

may be tempting to calculate $\sigma = \sqrt{\sigma_x^2 + \sigma_y^2}$ and compare this value to the threshold obtained from (3). However, $\sigma_x^2 + \sigma_y^2$ is the variance of the distribution of $x + y$, which can look very different from the distribution of $\sqrt{x^2 + y^2}$. Most notably, the domain of $x + y$ is $(-\infty, \infty)$ but the domain of $\sqrt{x^2 + y^2}$ is $[0, \infty)$.

In the general case where $\sigma_x$ and $\sigma_y$ are different, the distribution of $z$ follows the Hoyt distribution (Hoyt, 1947), which is also known as the Nakagami-q distribution (Tavares, 2010) (not to be confused with the Nakagami-r distribution (Nakagami, 1960)).

The Hoyt cumulative density function can be written as an infinite sum of incomplete gamma function of increasing order. In Ropokis, Rontogiannis, and Mathiopoulos (2008), an approach is shown which allows for the truncation of the infinite sum such that the truncation error is lesser than a predetermined threshold. In other words,

$$\mathrm{CDF}_{\mathrm{Hoyt}}(r) = \sum_{k=0}^{N} \frac{c_k}{\Gamma(k + n/2)} \gamma\left(\frac{n}{2} + k, \frac{r}{2\beta}\right) \tag{18}$$

where $\Gamma(\cdot)$ is the Gamma function, $\gamma$ is the lower incomplete Gamma function, and $n = 2$ the dimension of the system.

The scalar $\beta$ is defined in Ropokis et al. (2008) as:

$$\beta = \frac{2 \max_i \lambda_i \min_i \lambda_i}{\max_i \lambda_i + \min_i \lambda_i} \tag{19}$$

The scalar $c_k$ is defined as follows:

$$c_k = \frac{1}{2k} \sum_{l=0}^{k-1} d_{k-l} c_l \tag{20}$$

where

$$c_0 = \prod_{i=1}^{n} \left(\frac{\beta}{\lambda_i}\right)^{1/2} \tag{21}$$

$$d_k = \sum_{i=1}^{n} \left(1 - \frac{\beta}{\lambda_i}\right)^k \tag{22}$$

For the specific case of the two-dimensional distribution, it can be shown that

$$\beta = \frac{2\sigma_x^2 \sigma_y^2}{\sigma_x^2 + \sigma_y^2} = \frac{2\eta^2 \sigma^2}{1 + \eta^2} \tag{23}$$

where $\eta = \sigma_y / \sigma_x$ is the ratio of the smaller and larger standard deviations (i.e. $0 \leq \eta \leq 1$). The two standard deviations are rewritten as a single standard deviation and a scale factor because the scale factor more succinctly captures the relative information available along the two principal axes. When $\eta$ is close to 1, this implies that the estimator is able to provide similar uncertainty bounds

along both of the principal axes and points to the information content in the map being similar in both directions. However, when $\eta$ is close to 0, it implies that almost all of the observability is along the first principal axis.

The inverse of the summation of a series of incomplete Gamma function is not trivial; therefore (18) is not particularly useful in deriving the standard deviation bound for meeting the radial error threshold statistic. For this reason, an approximation approach developed by Tavares (2010) is chosen in the present work. The approach in that reference approximates the infinite sum using Gauss-Chebyshev quadrature. The number of terms which is required to ensure that the approximation error does not exceed a given bound can be calculated beforehand. The Tavares approximation for the Hoyt cumulative density function is given by:

$$\begin{aligned}\mathrm{CDF}_{\mathrm{Hoyt}}(r) =& 1 - \frac{2q}{n\left(1+q^2\right)} \sum_{k=1}^{n} \frac{\exp\left[-\frac{\left(1+q^2\right)^2}{4q^2} g(q,k,n)\, \frac{r^2}{\Omega}\right]}{g(q,k,n)} \\ &+ E_n\left(q, \frac{r}{\sqrt{\Omega}}\right)\end{aligned} \tag{24}$$

where Espinosa (2019) shows that $q$ is equal to the ratio of minimum and maximum standard deviations:

$$q = \frac{\min(\sigma_x, \sigma_y)}{\max(\sigma_x, \sigma_y)} = \eta \tag{25}$$

and $\Omega$ is the mean of the quadratic form (Provost & Mathai, 1992):

$$\Omega = \sigma_x^2 + \sigma_y^2 = \sigma^2(1+\eta^2) \tag{26}$$

The function $g(q,k,n)$ is defined in Tavares (2010) as follows:

$$\begin{aligned} g(q,k,n) &= 1 + \frac{1-q^2}{1+q^2} \cos\left(\pi \frac{2k-1}{2n}\right) \\ \text{or,} \quad g(\eta,k,n) &= 1 + \frac{1-\eta^2}{1+\eta^2} \cos\left(\pi \frac{2k-1}{2n}\right) \end{aligned} \tag{27}$$

and $E_n$ is the error associated with truncating the series at $n$ terms, given by:

$$\left| E_n\left(q, \frac{r}{\sqrt{\Omega}}\right)\right| \leq |E_n(q,0)| = \frac{2}{\left(\frac{1+q}{1-q}\right)^{2n} + 1} = \frac{2}{\left(\frac{1+\eta}{1-\eta}\right)^{2n} + 1} \tag{28}$$

From (25), $\eta$ is known beforehand (typically from the estimator), so the number of terms $n$ required

to meet a given tolerance $\varepsilon$ can be obtained by solving (28):

$$n = \text{ceil}\left[\frac{1}{2}\log\left(\frac{2}{\varepsilon} - 1\right)\Big/\log\left(\frac{1+\eta}{1-\eta}\right)\right] \tag{29}$$

A reasonable choice for the tolerance $\varepsilon$ is some fraction of the probability of exceedance. Once $n$ has been determined from (29), the equation that needs to be solved for a given containment radius and probability of exceedance of that limit is given by:

$$\text{CDF}_{\text{Hoyt}}(r_t, \sigma, \eta) = 1 - p_e \tag{30}$$

This equation can be solved for $\sigma$ by using the truncated sum of terms in (24):

$$\begin{aligned} &\frac{2\eta}{n\,(1+\eta^2)} \sum_{k=1}^{n} \frac{\exp\left[-\dfrac{\left(1+\eta^2\right)^2}{4\eta^2} g(\eta,k,n)\, w\right]}{g(\eta,k,n)} = p_e \\ &w = \frac{r_t^2}{\sigma^2(1+\eta^2)} \end{aligned} \tag{31}$$

Since (31) is nonlinear in $\sigma$, Newton-Raphson iteration is proposed as an alternative to direct solution:

1. Initialize $\hat{w}$ with the variance calculated from the Rayleigh threshold in (7):

$$\hat{w} = \frac{r_t^2}{\sigma^2(1+\eta^2)} = -\frac{2\log p_e}{1+\eta^2} \tag{32}$$

2. Calculate the function $f(\hat{w})$ which is given by (31):

$$f(\hat{w}) = \frac{2\eta}{n\,(1+\eta^2)} \sum_{k=1}^{n} \frac{\exp\left[-\dfrac{\left(1+\eta^2\right)^2}{4\eta^2} g(\eta,k,n)\, \hat{w}\right]}{g(\eta,k,n)} \tag{33}$$

3. Calculate $f'(\hat{w})$, which is the derivative of $f(w)$ with respect to $w$ and evaluated at $\hat{w}$:

$$f'(\hat{w}) = \left.\frac{\partial f(w)}{\partial w}\right|_{w=\hat{w}} = -\frac{\left(1+\eta^2\right)}{2n\eta} \sum_{k=1}^{n} \exp\left[-\frac{\left(1+\eta^2\right)^2}{4\eta^2} g(\eta,k,n)\, \hat{w}\right] \tag{34}$$

4. Calculate a correction $\Delta w$ from the following:

$$\Delta w = \frac{p_e - f(\hat{w})}{f'(\hat{w})} \tag{35}$$

5. Calculate $\hat{w}' = \hat{w} + \Delta w$

6. If $|f(\hat{w}') - f(\hat{w})| > \varepsilon$ then update $\hat{w} \leftarrow \hat{w}'$ and repeat Steps (2) through (5), otherwise calculate $\sigma$ from (31):

$$\sigma = \sqrt{\frac{r_t^2}{\hat{w}(1+\eta^2)}} \tag{36}$$

The computation of uncertainty bounds from the Hoyt distribution is generally well-behaved except for limiting cases when $\eta \to 1$, or when $\eta \to 0$. These are discussed in the following subsections.

### 3.1 Limiting Case: $\eta \to 1$

When $\eta = 1$, the denominator in (29) is indeterminate; however, the limit still exists, and it can be shown that $n = 1$. With $n = 1$ and $q = \eta = 1$, it can be shown that the Gauss-Chebyshev quadrature form of (24) is identical to the Rayleigh distribution in (5). Therefore, (7) can be used in this specific case.

It can be observed that for a given tolerance $\varepsilon$, $n$ is a decreasing function of $\eta$ with a minimum value of 1. The calculation of the number of terms in Gauss-Chebyshev quadrature can be safe-guarded by ensuring that $n$ is at least equal to 1 when $\eta$ is greater than some threshold value $\eta_{\max}$, which is given by solving (29) with $n = 1$:

$$\begin{aligned} & \log\left(\frac{1+\eta_{\max}}{1-\eta_{\max}}\right) = \frac{1}{2}\log\left(\frac{2}{\varepsilon} - 1\right) \\ \text{or,} \quad & \frac{1+\eta_{\max}}{1-\eta_{\max}} = \exp\left[\frac{1}{2}\log\left(\frac{2}{\varepsilon} - 1\right)\right] \\ \Rightarrow \quad & \eta_{\max} = \frac{\exp\left[\frac{1}{2}\log\left(\frac{2}{\varepsilon} - 1\right)\right] - 1}{\exp\left[\frac{1}{2}\log\left(\frac{2}{\varepsilon} - 1\right)\right] + 1} = \frac{\sqrt{\frac{2}{\varepsilon} - 1} - 1}{\sqrt{\frac{2}{\varepsilon} - 1} + 1} \end{aligned} \tag{37}$$

For example, when the required tolerance is $\varepsilon = 10^{-9}$, then (37) shows that the limiting ratio is equal to $\eta_{\max} = 0.9999553$; so if $\eta$ is larger than this value, one can use the Rayleigh distribution without any concern for overestimating the bound within the accuracy limits.

### 3.2 Limiting Case: $\eta \to 0$

When $\eta$ approaches 0, the number of terms required to calculate the sum in (24) approaches infinity because the denominator in (29) approaches zero. However, in the limiting case, when $\eta = 0$, the two-dimensional distribution collapses into a one-dimensional distribution where the threshold requirement is given by $\text{CDF}(|x| \leq r_t) = 1 - p_e$. This cumulative density function corresponds to the one-sided Gaussian distribution or half-normal distribution and can derived from the two-sided Gaussian distribution cumulative density function. In fact the value of $\sigma$ can be calculated by

allowing $\sigma_y \to \infty$ in (12), for which the value of the error function approaches unity. Consequently,

$$\text{erf}\left(\frac{r_t}{\sqrt{2}\,\sigma}\right) = 1 - p_e \tag{38}$$

which can be solved as shown below:

$$\sigma = \frac{r_t}{\sqrt{2}\text{erf}^{-1}\left(1 - p_e\right)} \tag{39}$$

Let the maximum number of terms allowed in the quadrature formula be denoted by $n_{\max}$. For a given error tolerance $\varepsilon$, the lower bound on $\eta$, denoted by $\eta_{\min}$ can be obtained by solving (29). This value is given by:

$$\eta_{\min} = \frac{\left(\frac{2}{\varepsilon} - 1\right)^{1/(2n_{\max})} - 1}{\left(\frac{2}{\varepsilon} - 1\right)^{1/(2n_{\max})} + 1} \tag{40}$$

Therefore if $\eta < \eta_{\min}$ the one-sided Gaussian solution in (39) should be used.

## 4 Results and Analysis

Figure 7 shows a comparison of the one-sided Gaussian (circles), Hoyt (squares), and Rayleigh distributions (diamonds). Comparison is made by plotting the probability exceedance, or survival function, i.e. one minus the cumulative density, on a log scale. As discussed earlier, the one-sided Gaussian is the limiting distribution when the ratio of standard deviations along the minor and major axis approaches zero, and the Rayleigh distribution is the limiting distribution when the ratio of standard deviations approaches one (i.e. both standard deviations are equal). The value used to generate Figure 7 is $\eta = 0.8$. The figure also shows that the Hoyt distribution calculated using quadratures agrees closely with the Hoyt distribution calculated using the truncated sum of weighted incomplete gamma functions: the differences are on the order of $10^{-13}$ as depicted by the dashed line.

In Table 1, the Hoyt distribution is used to calculate the thresholding standard deviation $\sigma_{\text{limit}_{\text{Hoyt}}}$ for $r_t = r_{\text{RNP}}$, i.e. a probability of exceedance of 0.05. The implementation listed in (24) through (36) is used to calculate this value to an error tolerance of $10^{-12}$, and the table lists the standard deviation value scaled by $r_{\text{RNP}}$ in order to nondimensionalize the answer. In the third column of Table 1, the limiting standard deviation from the Hoyt distribution is divided by the standard deviation of the Rayleigh distribution, which is equal to $0.408\,r_{\text{RNP}}$ as shown in (8). This demonstrates the potential benefit of using a Hoyt distribution for radial error characterization in MagNav. For example, when the standard deviation along the minor axis of the covariance ellipse is an order of magnitude smaller than the standard deviation along the major axis, then $\eta \approx 0.1$.

In general it is observed that when the principal axis standard deviations are even moderately different, e.g. the ratio of the smaller standard deviation to the larger standard deviation is 0.5 or lower, the requirement driving a larger standard deviation can be relaxed by more than 20% if the 95th percentile bound is applied on the radial error distribution instead of the error distribution along a single axis. This can allow more flexibility in navigation filter design by removing the need to tune the filter for better accuracy on each axis and instead require tuning to reduce the radial error only. Conversely, this also means that a 95% accuracy requirement on the radial error leads to a stronger guarantee on separation assurance.

An argument can be made to use a modified version of the formulation in (12) using $\sigma_x = \sigma$ and $\sigma_y = \eta\sigma$:

$$\operatorname{erf}\left(\frac{r_t}{\sqrt{2}\,\sigma}\right)\operatorname{erf}\left(\frac{r_t}{\sqrt{2}\,\eta\sigma}\right) = 1 - p_e \tag{41}$$

The foregoing equation can be solved by Newton-Raphson iteration in order to calculate $\sigma$ but assumes that numerical implementations of the error function and its inverse are available. It should be noted, however, that the (41) is applying a constraint on the infinity norm of the two-dimensional position error, and not on the radial error (two-norm of the error). For a two-dimensional random variable $z$, the area covered by the inequality $||z_||_\infty \leq r_t$ is always greater than the area covered by the inequality $||z||_2 \leq r_t$. Consequently, $p(||z||_\infty \leq r_t) \geq p(||z||_2 \leq r_t)$, and the probability of exceeding $r_t$ follows $p(||z||_\infty > r_t) < p(||z||_2 > r_t)$. It follows that applying the RNP accuracy condition on the infinity norm does not provide any meaningful bound on the radial error.

The results from Table 1 are generalized to a range of exceedance probabilities and are shown in Figure 8. In this figure, level curves are shown for a combination of ratio of principal major and minor axis stand deviations along the x axis) and probability of exceedance on the y axis, using a log scale. As $\eta$ increases, the bounding standard deviation from the Hoyt distribution approaches the value obtained from the Rayleigh distribution, as expected. This means that for sufficiently high ratios, the penalty incurred by using a Rayleigh approximation is sufficiently low to not result in any meaningful benefit by using a Hoyt distribution. This also holds true for sufficiently low probabilities of exceedance. For example, containment region statistics which require a probability of exceedance of $10^{-7}$ can still use a Rayleigh approximation with a penalty of a 5% over-estimate on the limiting $\sigma$ value.

Finally, Figure 9 shows the number of Newton-Raphson iterations required in order to calculate the bounding standard deviation numerically, when the required tolerance is equal to $10^{-12}$. This is a function of both the ratio $\eta$ as well as the probability of exceedance, but in all cases, the total number of iterations required is limited to 12. It is worth noting that the limit reduces to 8 if the required tolerance is $10^{-10}$. In the event computational requirements limit the number of iterations possible, the gradient calculation in (34) can be used to obtain a first-order correction to the Rayleigh distribution. The approximation error due to this limit has not been evaluated in this paper.

# 5 Conclusions

The integration of magnetic navigation in civil aviation operations requires adapting concepts such as RNP from current GPS-based navigation. The definition of RNP and similar accuracy metrics draws from statistical analysis where the probability of exceedance values are derived from the standard deviations of one-dimensional normal distributions. Since the use of magnetic navigation does not always adhere to the assumptions that are used to define RNP and similar statistics, a thorough analysis has been performed in this paper which quantifies the errors incurred while making these assumptions. This paper develops a radial error model based on the Hoyt distribution which more rigorously adheres to the spirit of the RNP and similar navigation accuracy definitions. Since the Hoyt distribution probability density function and cumulative density function and its inverses are not easy to model using elementary functions, this paper concurrently develops robust numerical methods in order to evaluate these functions and to make the computation tractable. With the robust, explainable, and computationally tractable nature of this approach, the paper suggests that the radial error statistic is well suited for defining navigation accuracy in civil aviation.

## References


Abramowitz, M., & Stegun, I. A. (1972). *Handbook of mathematical functions with formulas, graphs, and mathematical tables* (10th ed.). Marcel Dekker.

Blanch, J., Walter, T., Enge, P., Lee, Y., Pervan, B., Rippl, M., Spletter, A., & Kropp, V. (2015). Baseline advanced RAIM user algorithm and possible improvements. *IEEE Transactions on Aerospace and Electronic Systems*, *51*(1), 713-732. https://doi.org/10.1109/TAES.2014.130739

Canciani, A. J. (2022). Magnetic navigation on an F-16 aircraft using online calibration. *IEEE Transactions on Aerospace and Electronic Systems*, *58*(1), 420–434. https://doi.org/10.1109/TAES.2021.3101567

Canciani, A. J., & Raquet, J. F. (2016). Absolute positioning using the earth's magnetic anomaly field. *NAVIGATION*, *63*(2), 111-126. https://doi.org/10.1002/navi.138

Crassidis, J. L., & Junkins, J. L. (2004). *Optimal estimation of dynamical systems.* Chapman & Hall.

Espinosa, P. R. (2019). *Analysis of Gaussian quadratic forms with application to statistical channel modeling* [PhD Thesis, Universidad de Málaga]. https://hdl.handle.net/10630/19450

Federal Aviation Administration. (2024). *2024 Federal Aviation Regulations/Aeronautical Information Manual.* Aviation Supplies & Academics.

Gnadt, A. R. (2022a). *Advanced aeromagnetic compensation models for airborne magnetic anomaly navigation* [PhD Thesis, Massachusetts Institute of Technology]. https://hdl.handle.net/1721.1/145137

Gnadt, A. R. (2022b). Machine learning-enhanced magnetic calibration for airborne magnetic anomaly navigation. In *AIAA SCITECH 2022 Forum.* https://doi.org/10.2514/6.2022-1760

Gnadt, A. R., Belarge, J., Canciani, A., Carl, G., Conger, L., Curro, J., Edelman, A., Morales, P., Nielsen, A. P., OKeeffe, M. F., Rackauckas, C. V., Taylor, J., & Wollaber, A. B. (2023). *Signal enhancement for magnetic navigation challenge problem.* https://arxiv.org/abs/2007.12158

Gnadt, A. R., Wollaber, A. B., & Nielsen, A. P. (2022). *Derivation and extensions of the Tolles-Lawson model for aeromagnetic compensation.* https://arxiv.org/abs/2212.09899

Gupta, A., Sengupta, P., Phernetton, R., & Sosanya, A. (2024). Lower bounds on magnetic navigation performance as a function of magnetic anomaly map quality. In *2024 AIAA DATC/IEEE 43rd Digital Avionics Systems Conference (DASC)* 1–7. https://doi.org/10.1109/DASC62030.2024.10749342

Hoyt, R. S. (1947). Probability functions for the modulus and angle of the normal complex variate. *The Bell System Technical Journal*, *26*(2), 318–359. https://doi.org/10.1002/j.1538-7305.1947.tb01318.x

ICAO doc 9613, performance-based navigation (PBN) manual (5th ed.). (2023). International Civil Aviation Organization.

Langley, R. B. (1999). Dilution of precision. *GPS World*, *10*(5), 52-59.

Maus, S., Barckhausen, U., Berkenbosch, H., Bournas, N., Brozena, J., Childers, V., Dostaler, F.,

Fairhead, J. D., Finn, C., von Frese, R. R. B., Gaina, C., Golynsky, S., Kucks, R.,Lühr, H., Milligan, P., Mogren, S., Müller, R. D., Olesen, O., Pilkington, M., ... Caratori Tontini, F. (2009). EMAG2: A 2arc min resolution Earth magnetic anomaly grid compiled from satellite, airborne, and marine magnetic measurements. *Geochemistry, Geophysics, Geosystems*, *10*(8). https://doi.org/https://doi.org/10.1029/2009GC002471

Moradi, M., Zhai, Z.-M., Nielsen, A., & Lai, Y.-C. (2024). Random forests for detecting weak signals and extracting physical information: A case study of magnetic navigation. *APL Machine Learning*, *2*(1), 016118. https://doi.org/10.1063/5.0189564

Nakagami, M. (1960). The m-distribution a general formula of intensity distribution of rapid fading. In W. C. Hoffman (Ed.), *Statistical Methods in Radio Wave Propagation* (pp. 3–36). Pergamon. https://doi.org/10.1016/B978-0-08-009306-2.50005-4

Nerrise, F., Sosanya, A. S., & Neary, P. (2024). *Physics-informed calibration of aeromagnetic compensation in magnetic navigation systems using liquid time-constant networks.* https://arxiv.org/abs/2401.09631

North American Magnetic Anomaly Group. (2002). *Magnetic anomaly map of North America.* U.S. Geological Survey. https://doi.org/10.3133/70211067

Phillips, J. D. (2005). Potentialfield continuation: Past practice vs. modern methods. In *SEG Technical Program Expanded Abstracts 1996* (pp. 1411-1414). https://doi.org/10.1190/1.1826376

Provost, S. B., & Mathai, A. M. (1992). *Quadratic forms in random variables: Theory and applications*. Marcel Dekker.

Ropokis, G. A., Rontogiannis, A. A., & Mathiopoulos, P. T. (2008). Quadratic forms in normal RVs: theory and applications to OSTBC over Hoyt fading channels. *IEEE Transactions on Wireless Communications*, *7*(12), 5009–5019. https://doi.org/10.1109/T-WC.2008.070830

Saltus, R. W., Chulliat, A., Meyer, B., Bates, M., & Sirohey, A. (2023). Magnetic anomaly grid and associated uncertainty from marine trackline data: The Caribbean Alternative Navigation Reference Experiment (CANREx). *Earth and Space Science*, *10*(11), e2023EA002958. https://doi.org/https://doi.org/10.1029/2023EA002958

SC-159. (2020a). *DO229F: Minimum operational performance standards (MOPS) for global positioning system/satellite-based augmentation system airborne equipment.* RTCA, Inc.

SC-159. (2020b). *DO384: Minimum operational performance standards (MOPS) for GNSS aided inertial systems.* RTCA, Inc.

Tavares, G. N. (2010). Efficient computation of Hoyt cumulative distribution function. *Electronics Letters*, *46*, 537–539. https://doi.org/10.1049/el.2010.0189

Tkhorenko, M., & Karshakov, E. (2022). Estimating the potential accuracy of magnetic navigation based on magnetic survey data. In *2022 29th Saint Petersburg International Conference on Integrated Navigation Systems (ICINS)* (p. 1-3). https://doi.org/10.23919/ICINS51784.2022.9815357

Zhai, Z.-M., Moradi, M., Kong, L.-W., & Lai, Y.-C. (2023). Detecting weak physical signal from noise: A machine-learning approach with applications to

magnetic-anomaly-guided navigation. *Physical Review Applied*, *19*, 034030. https://doi.org/10.1103/PhysRevApplied.19.034030

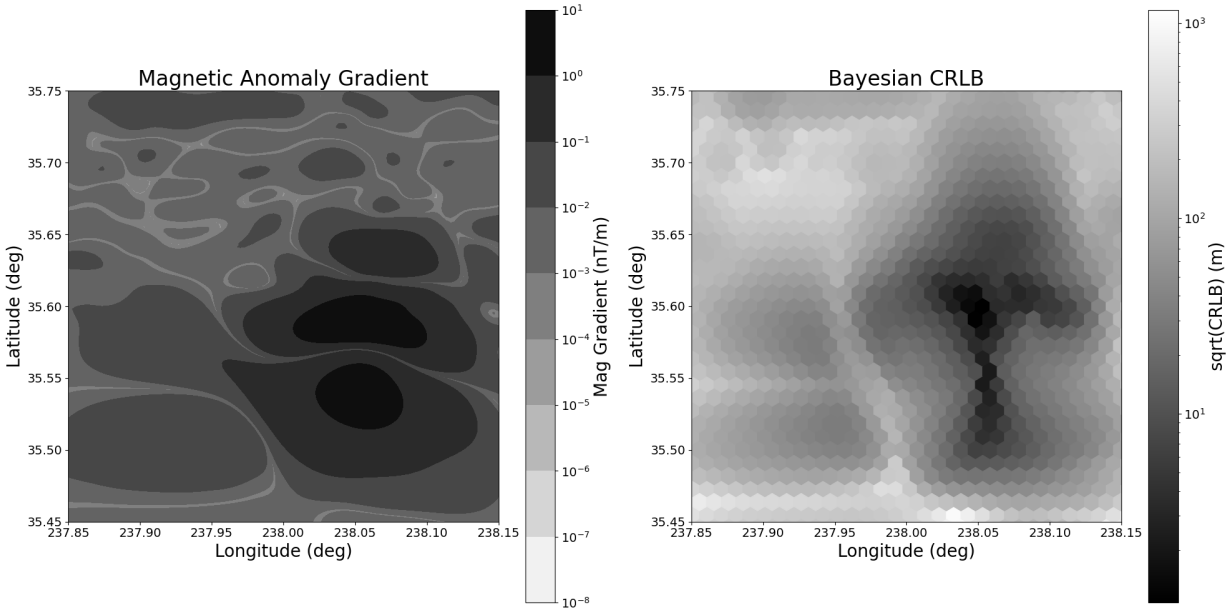


Figure 1: Magnetic Anomaly and Cramer-Rao Lower Bound, Heading = 0 deg.

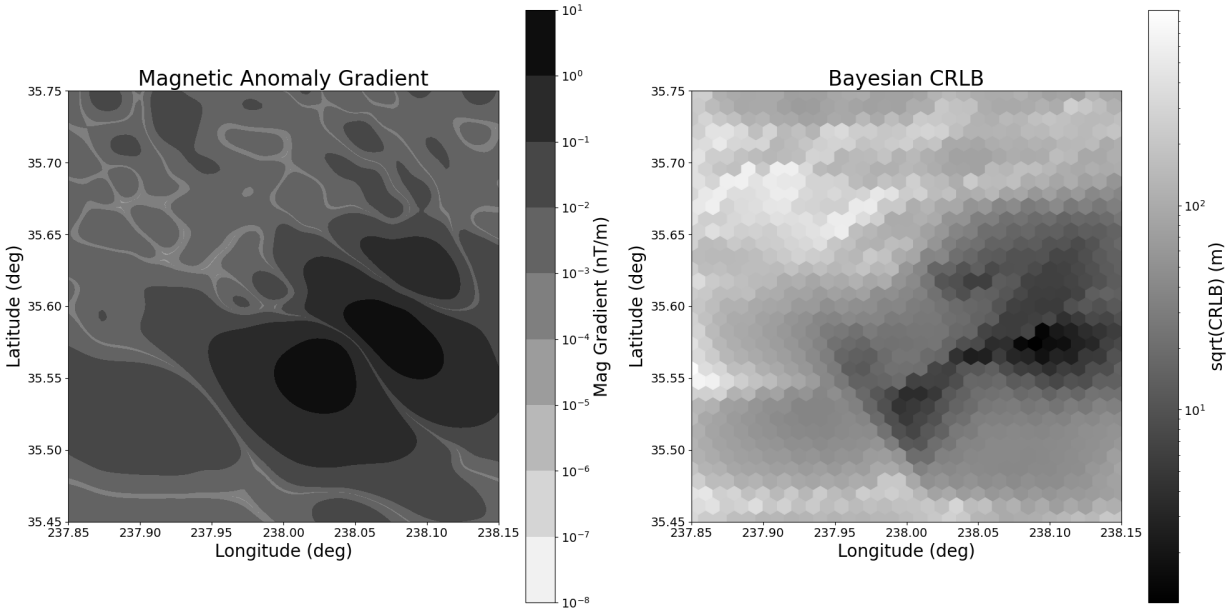


Figure 2: Magnetic Anomaly and Cramer-Rao Lower Bound, Heading = 60 deg.

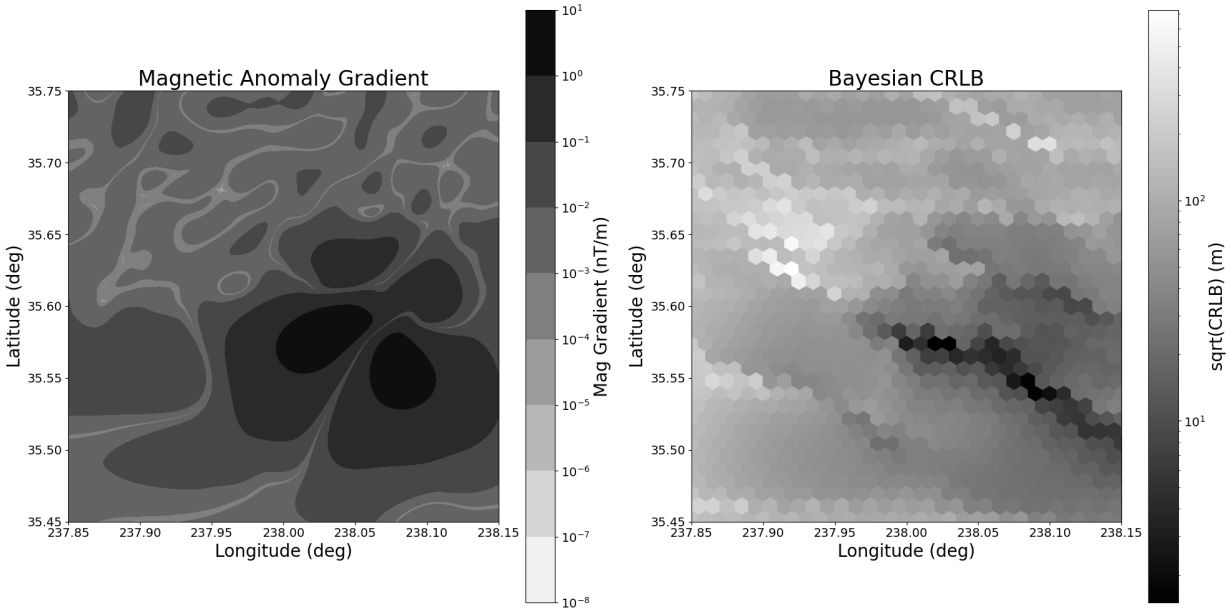


Figure 3: Magnetic Anomaly and Cramer-Rao Lower Bound, Heading = 120 deg.

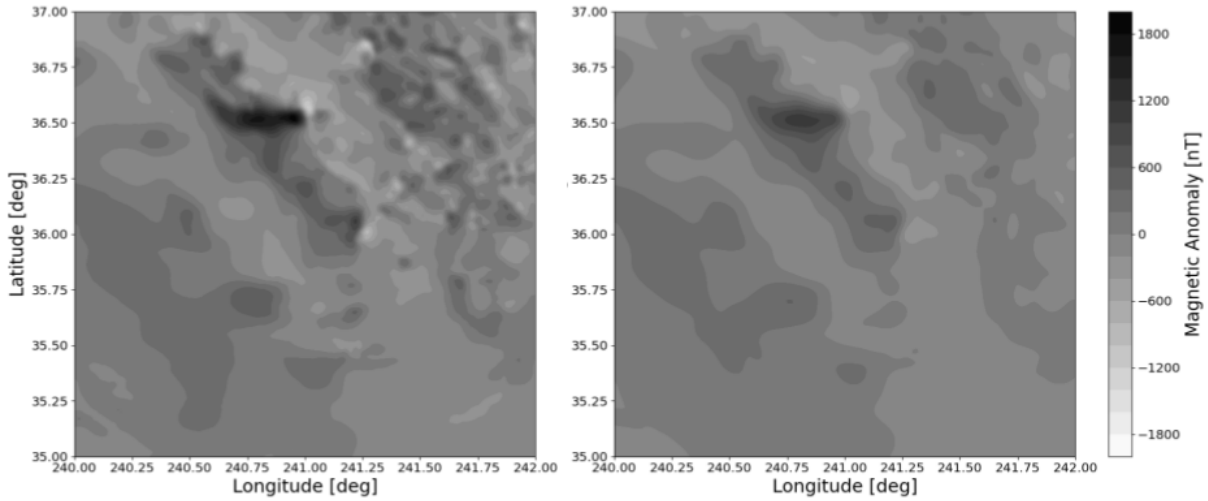


Figure 4: Magnetic Anomaly at 1000 m (left) and 4000 m (right)

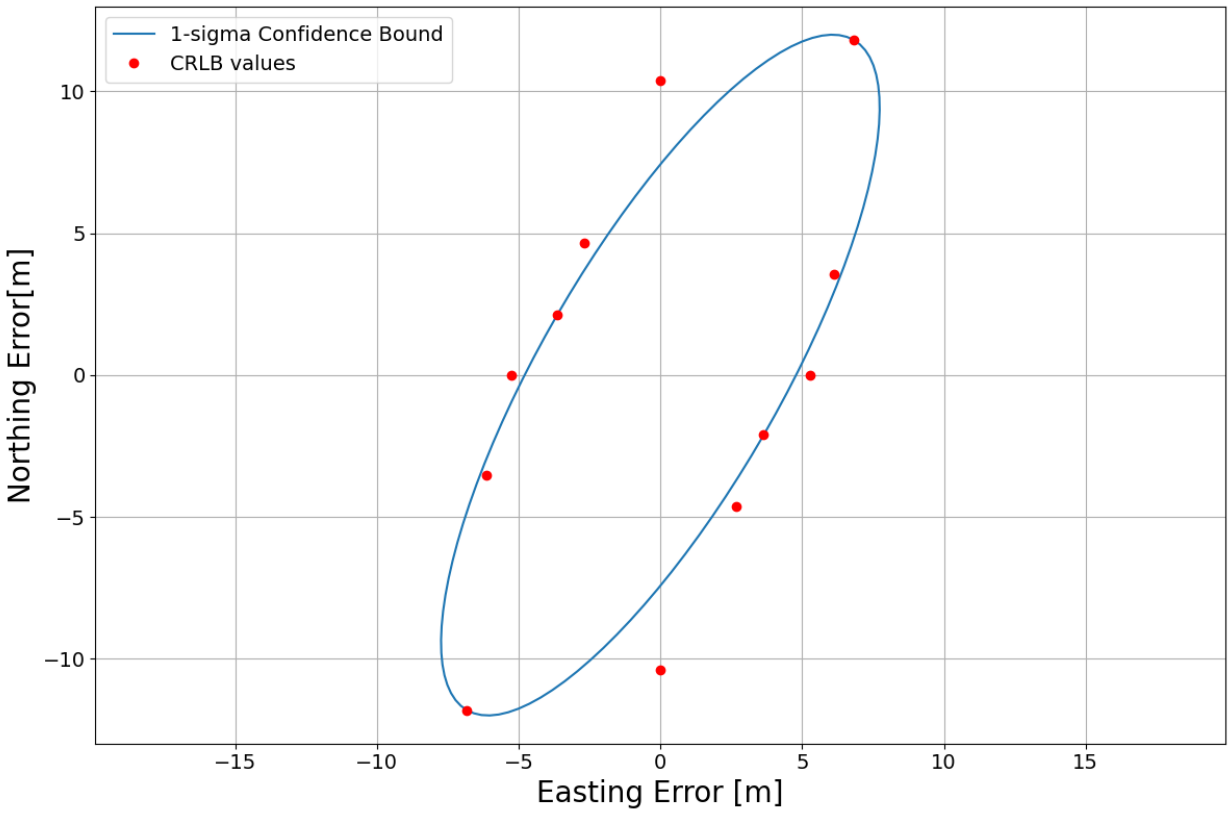


Figure 5: Confidence Lower-Bound at location Latitude = 35.6°N, Longitude = 238.1° (121.9°W)

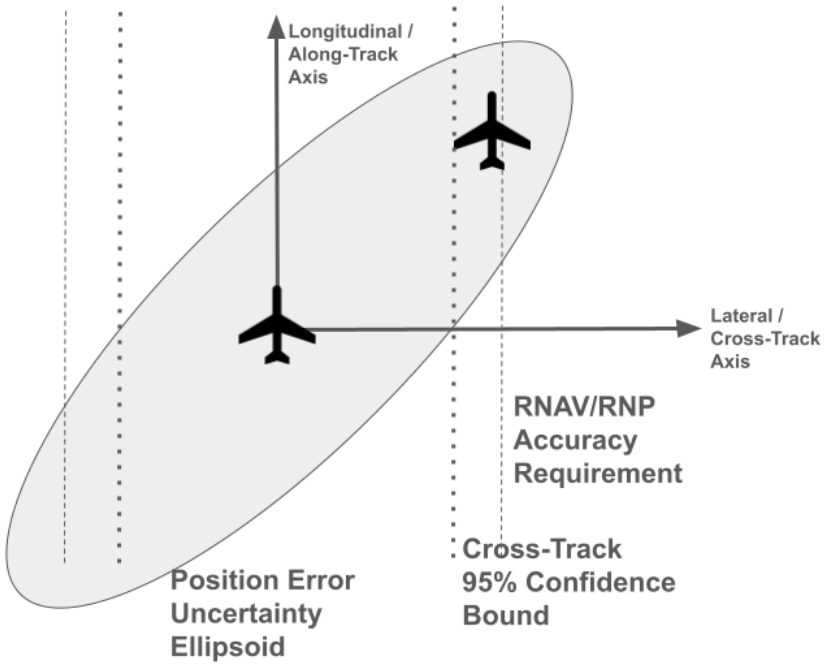


Figure 6: General Position Error Uncertainty from Magnetic Navigation and the Impact on Accuracy Specifications.

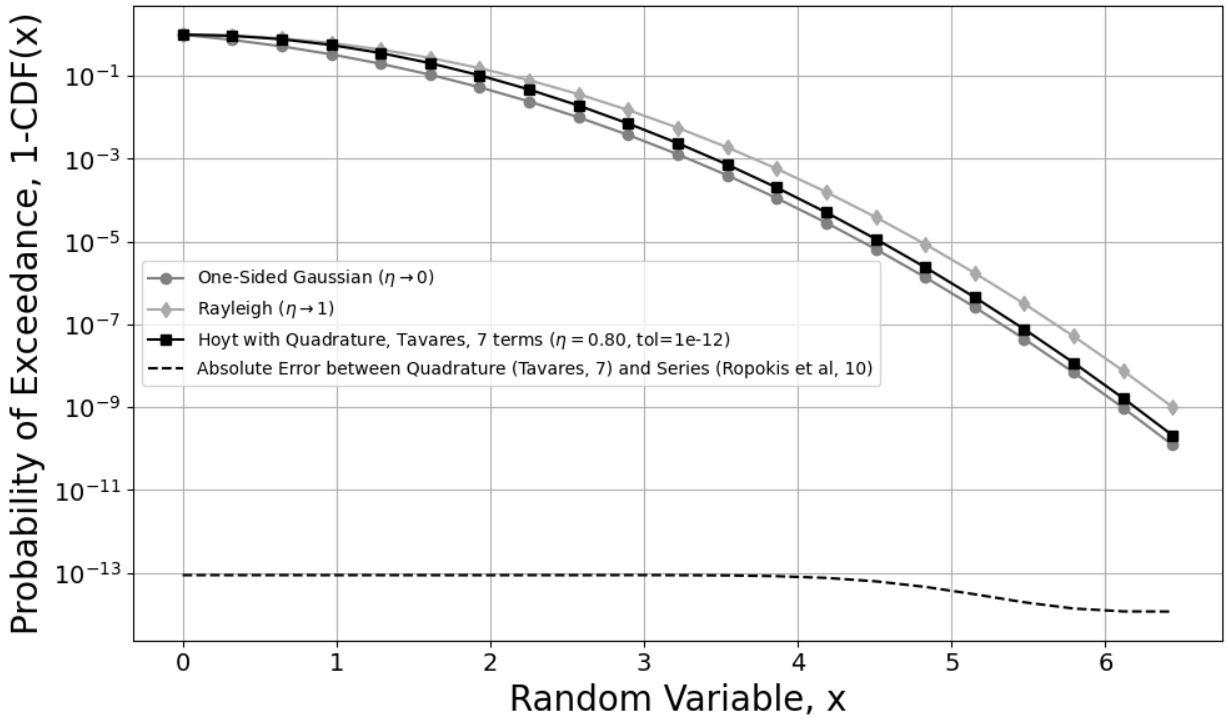


Figure 7: Comparison of Probability of Exceedance for One-Sided Gaussian, Hoyt, and Rayleigh Distributions.

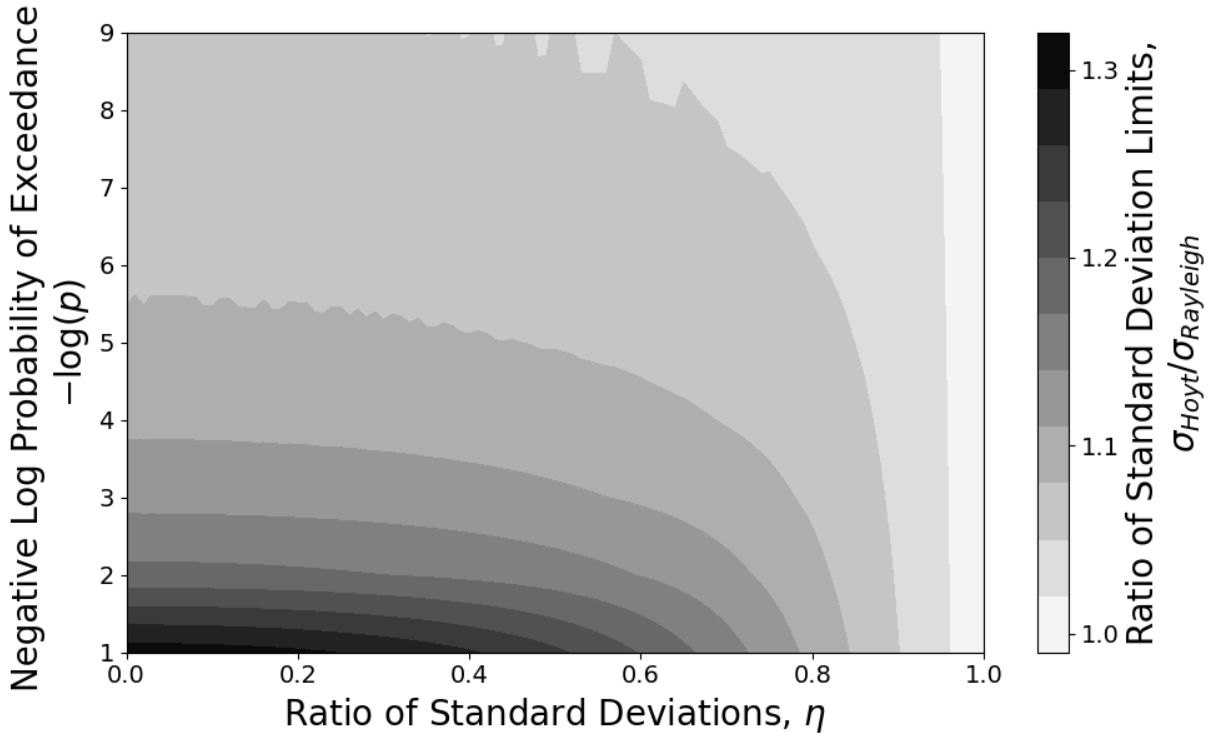


Figure 8: Ratio of Standard Deviation Limits Obtained from Hoyt and Rayleigh Distributions for Different Probabilities of Exceedance

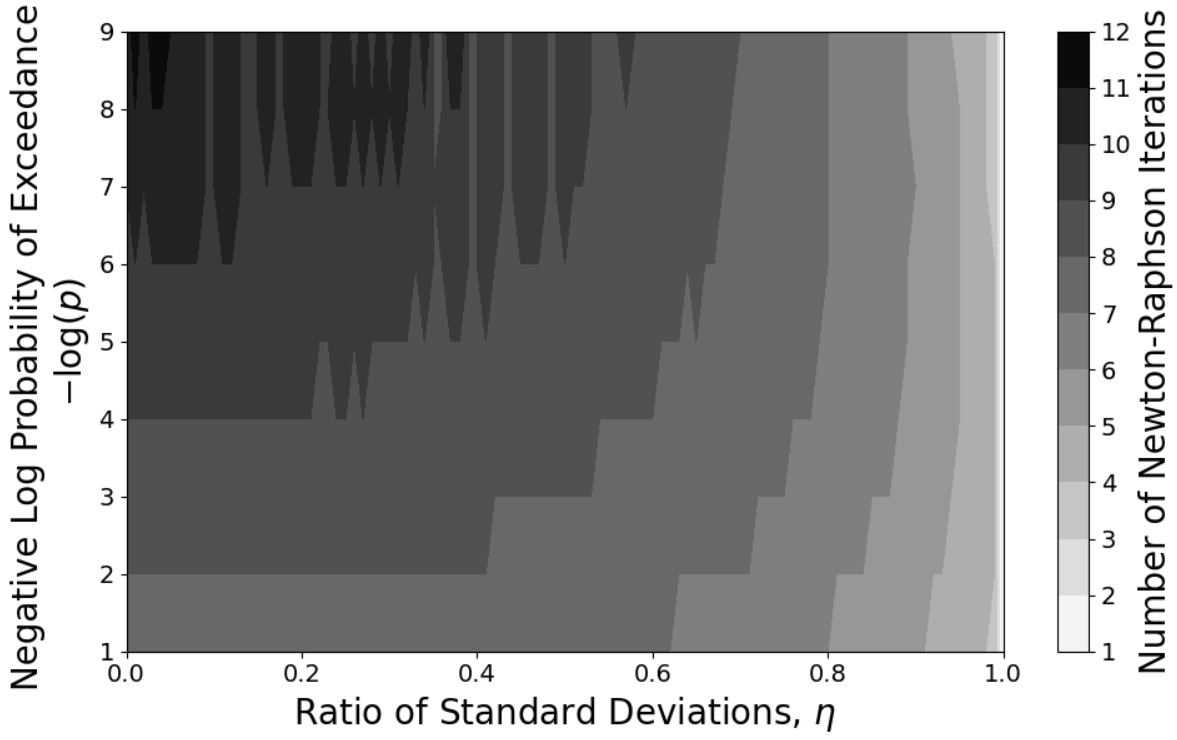


Figure 9: Number of Newton-Raphson Iterations Required.

| Ratio of Standard Deviations $\eta = \sigma_y/\sigma_x$ | Principal Axis Standard Deviation $\sigma_{\text{limit}_{\text{Hoyt}}}/r_{\text{RNP}}$ | Increase Factor $\sigma_{\text{limit}_{\text{Hoyt}}}$ / $\sigma_{\text{limit}_{\text{Rayleigh}}}$ |
|---|---|---|
| 0.01 | 0.510 | 1.25 |
| 0.1 | 0.510 | 1.25 |
| 0.2 | 0.508 | 1.24 |
| 0.3 | 0.504 | 1.23 |
| 0.4 | 0.499 | 1.22 |
| 0.5 | 0.491 | 1.20 |
| 0.6 | 0.480 | 1.18 |
| 0.7 | 0.466 | 1.14 |
| 0.8 | 0.448 | 1.10 |
| 0.9 | 0.429 | 1.05 |
| 0.99 | 0.411 | 1.00 |

Table 1: RNP Requirement Relaxation with Hoyt Distribution.